www.sciencemag.org/content/351/6274/703/suppl/DC1

Supplementary Materials for

Artificial electron acceptors decouple archaeal methane oxidation from sulfate reduction

Silvan Scheller,* Hang Yu, Grayson L. Chadwick, Shawn E. McGlynn, Victoria J. Orphan*

*Corresponding author. E-mail: vorphan@gps.caltech.edu (V.J.O.); scheller@caltech.edu (S.S.)

Published 12 February 2016, *Science* **351**, 703 (2016)
DOI: 10.1126/science.aad7154

This PDF file includes:

Materials

Sediment collection and processing

Santa Monica basin seep sediments overlain by a white mat were collected from the Santa Monica Mounds site in a push core (PC 61) deployed by the ROV *Doc Ricketts.* Samples were collected in May 2013 during a research cruise organized by the Monterey Bay Aquarium Research Institute (MBARI) using the R/V *Western Flyer*. PC61 was collected during dive 463 at 860 m depth with an *in situ* temperature of 4 °C (lat. 33.78905, long. -118.66833). The intact sediment core was extruded shipboard and then heat-sealed in a large mylar bag flushed for 5 minutes with argon. Sediments were stored at 4 °C until processed in the lab (40 days after collection). The whole push core (ca. 12 cm, yielding 800 ml wet sediment) was suspended in 1600 ml filter sterilized N_2 sparged bottom seawater from the site (1 in 3 ratio) in an anaerobic chamber (3% H_2 in N_2). The anaerobic sediment slurry was then distributed into three 1L pyrex bottles, sealed with a large butyl rubber stopper, and pressurized with methane (0.25 MPa). Aggregate counts at the start of the experiment were determined by DAPI staining and epifluorescence microscopy, yielding approximately 9.7 x 10^5 aggregates per ml wet weight sediment. The initial sulfate-coupled AOM activity of the sediment was assessed via sulfide production measurements, showing the generation of 2.8 mM sulfide within the first 15 days.

All manipulations of the sediment incubations were done anaerobically at 4 °C or on ice. Prior to establishment of the microcosm experiments, the seep sediment was maintained for 12 months at 4 °C under methane (0.25 MPa) in anoxic bottom seawater that was exchanged every 3 months. For all reported experiments in this study, the seawater above the sediment was exchanged with a modified artificial seawater (see below) that contained 10x less Ca^{2+}, no sulfate, no sulfide, and 25 mM HEPES buffer at pH 7.5. The low Ca^{2+} concentration and lower pH prevent carbonate precipitation, which allows quantitative analysis of the ^{13}C-bicarbonate formed in solution during ^{13}C-methane oxidation. Methane was added (0.30 MPa), shaken and the sediment allowed to settle for 48 hours (sediment/total volume = 1:3). The supernatant was exchanged 3 times with the described medium following the same procedure in order to obtain sulfate and sulfide-free sediment.

Medium composition:

The final composition in the medium was: NaCl 457 mM, $MgCl_2$ 47 mM, Na^+-HEPES (pH=7.5) 25 mM, KCl 7.0 mM, $NaHCO_3$ 5.0 mM, $CaCl_2$ 1.0 mM, K_2HPO_4 1.0 mM, NH_4Cl 1.0 mM, SeO_3^{2-} 0.01 µM, WO_4^{2-} 0.007 µM, 0.1% trace element solution, containing per liter: nitrilotriacetic acid 150 mg, $MnCl_2$ x 4 H_2O 610 mg, $CoCl_2$ x 6 H_2O 420 mg, $ZnCl_2$ 90 mg, $CuCl_2$ x 2 H_2O 7 mg, $AlCl_3$ 6 mg, H_3BO_3 10 mg, Na_2MoO_4 x 2 H_2O 20 mg, $SrCl_2$ x 6 H_2O 10 mg, NaBr 10 mg, KI 70 mg, $FeCl_3$ x 6 H_2O 500 mg, $NiCl_2$ x 6 H_2O 25 mg. No vitamins, indicators, reducing agents, or other substances were added. The sulfate concentration of the final sediment slurry was below detection limit (< 10 µM). Before the start of the microcosm experiments, the sediment slurry was flushed with methane (ca. 20 min) to remove traces of sulfide. The presence of sulfide (e.g. 0.5 mM in previous studies (*16, 31*) can chemically reduce AQDS, preventing methane oxidation with AQDS (*16*). It is possible that under these conditions, AOM is inhibited

by the polysulfides formed from sulfide + AQDS rather than directly by reduced AQDS, as reduced AQDS was observed to accumulate in our experiments with no apparent inhibition of AOM (Table S1A).

Sediment characterization
AOM rates with sulfate (1.5 μmol methane (cm^3 wet sediment)$^{-1}$ d^{-1}, see main text) were comparable to active methane-seep sediments described previously (*31, 32*). The dominant groups of archaea included ANME-2a and ANME-2c based on Illumina Tag sequencing using the Earth Microbiome primer set (Fig. S4). FISH hybridization and aggregate counts based on DAPI staining yielded 47% (69 of 146 aggregates) ANME-2a affiliated consortia and 43% ANME-2c (47 of 109 DAPI stained aggregates). The remaining 10% of aggregates likely represented other ANME not targeted by the specific FISH probes or possibly weakly hybridized ANME-2a or 2c aggregates that were below detection by FISH.

Chemicals and reagents
AQDS (=2,6-AQDS, >98% purity) and Fe(III)-EDTA was purchased from Sigma. Humic acids (sodium salt, tech. batch no. 10121HA) were obtained from Aldrich. 2,7-AQDS and 1,5-AQDS (>98% purity) were purchased from TCI chemicals. The different AQDS isomers were found to contain variable amounts of residual sulfate as determined by Ion Chromatography: 11 μM sulfate per 10 mM AQDS; 176 μM sulfate per 10 mM 2,7-AQDS; 344 μM sulfate per 10 mM 1,5-AQDS. 1,5-AQDS was re-crystallized from boiling water to remove traces of sulfate present in the purchased product. Residual sulfate in the re-crystallized 1,5-AQDS: 13 μM per 10 mM 1,5-AQDS. 2,7-AQDS, AQDS and all other chemicals were used as received. 50 mM Fe(III)-citrate stock solution was prepared by dissolving 2.0 mmol citric acid in a small amount of DI water, followed by the addition of 1.0 mmol $FeCl_3$ x 6 H_2O and pH adjustment to pH = 7.5 with NaOH. The solution was then diluted to 50 mM ferric ions (20 ml final volume).

Methods for metabolic measurements

General description of methane oxidation measurements via ^{13}C-methane
Methane oxidation was quantified by determining the production of inorganic carbon ("CO_2"). Accurate quantification of the concentration of inorganic carbon formed from methane oxidation is challenging due to 4 main reasons:
1) Inorganic carbon is present as a mixture of CO_2(g) in the headspace, and CO_2(aq.), H_2CO_3, HCO_3^- or CO_3^{2-} in solution (dissolved inorganic carbon, DIC)
2) Inorganic carbon may also be produced from respiration of organic carbon sources other than methane
3) Inorganic carbon can also be slowly produced via dissolution of carbonates (a major component of seep sediments)
4) Inorganic carbon may also precipitate with divalent cations as insoluble carbonates

For our experiments, we found that quantifying methane oxidation using the stable isotope tracer $^{13}CH_4$ in incubations with a known amount of unlabelled (dissolved inorganic carbon, DIC) by analyzing the ^{13}C enrichment in DIC was the most accurate

(Fig. S2A).We used a defined amount of added DIC in artificial, buffered seawater with a low calcium concentration to prevent carbonate precipitation (see medium composition). As $^{13}CH_4$ was the only ^{13}C-enriched carbon source added, the newly formed ^{13}C-DIC must be derived from methane. For low methane oxidation rates (less than ca. 5% relative to sulfate as the oxidant), however, enzyme-catalyzed isotope exchange between methane and DIC (*27, 28*), see also main text] needs to be taken into account, because it contributes to ^{13}C enrichment of the DIC without net methane oxidation, resulting in an overestimation of net methane oxidation. To illustrate the utility of this approach for quantifying rates of AOM, we used 2 AOM incubations amended with ^{13}C-methane and sulfate and compared our calculation of newly formed DIC based on $^{13}CH_4$ (Fig. S2B, red) with an independent method used in analytical chemistry based on standard addition that yields the absolute amounts of DIC formed during the incubations more directly (Fig. S2B, black). Details of both methods, the $^{13}CH_4$ experiments and the standard addition are described below. The method via standard addition provides evidence for net DIC increase during incubations, and is consistent with the progressive enrichment of ^{13}C-DIC observed from $^{13}CH_4$. In this comparative analysis, however, we observed an initial decrease in the absolute concentration of DIC within the first 2 days for the standard addition method, which we mainly attribute to diffusion of CO_2 into the headspace of the vial (Fig. S2B, black).

Incubation conditions for AOM rate measurement

Each incubation vial was set up with 1.0 cm^3 wet sediment (wet sediment = volume of sediment after allowing the sediment slurry settle for 48 h) in total slurry volume of 5 ml as follows: Sterile serum vials were closed with butyl rubber stoppers (volume = 12.9 ml after closing) and flushed with methane. 1.0 ml $^{13}CH_4$ (99% ^{13}C, Cambridge Isotope Laboratories, containing 0.05 vol% $^{13}CO_2$ as an impurity) was introduced anaerobically. 2.0 ml of artificial, anaerobic seawater containing 2.5x the target concentration of the corresponding electron acceptor was injected into the serum vial cooled on ice. For AQDS and 1,5-AQDS, this was a suspension corresponding to 25 mM (see Table S2). The 1L pyrex bottle with the sediment in the sulfate-free medium (1 part wet sediment in 3 parts of slurry volume) was vigorously shaken each time and 3.0 ml of slurry immediately removed and injected into the individual serum bottles. Each stoppered serum vial was supplemented with unlabelled methane (0.250 MPa overpressure: pressure gauge SSI Technologies, Inc., Media Gauge™), shaken and stored inverted at 4 °C (final headspace: 0.35 MPa methane, with ca. 4 % $^{13}CH_4$). The exact fractional abundance of ^{13}C in the methane was quantified via ^{1}H-NMR spectroscopy for individual incubations.

AOM rate measurements (quantification of newly formed DIC based on $^{13}CH_4$)

For ^{13}C-DIC analysis, 0.25 ml of the medium above the settled sediment in the microcosm was sampled with a disposable needle and syringe at each time point (same intervals for all experiments) and centrifuged (16000 rcf, 5 min). The supernatant was transferred into 0.6 ml eppendorf tubes, flash frozen in N_2(l), and stored at -20 °C until measurement. 150 µl of the thawed supernatant was then added to He-flushed vials containing 100 µl H_3PO_4 (85%). The resulting CO_2 was analyzed for the isotopic enrichment ($^{13}F(t_n)$) on a GC-IR-MS GasBench II (Thermo Scientific). The amount of

DIC newly formed ($\Delta[DIC](t_n)$, see Fig. 2B) was calculated from the measured ^{13}F (fractional abundance of ^{13}C), neglecting isotope effects on AOM:

$$\Delta[DIC](t_n) = [DIC](t_0) * (^{13}F(t_n) - {}^{13}F(t_0)) / (^{13}F(CH_4) - {}^{13}F(t_n))$$

[DIC] = sum of carbonate, bicarbonate and CO_2, $[DIC](t_0) = 5.0$ mM
$^{13}F(t_0) = 0.01153$ (higher than medium due to $^{13}CO_2$-impurity in the $^{13}CH_4$ used)
$^{13}F(CH_4) = {}^{13}C$ in the methane used (measured via ^{1}H-NMR spectroscopy)

Amount of DIC formed per vial (Fig. 1A, S1, S3) = 5 mL * $\Delta[DIC](t_n)$

Calculation of specific AOM rates per volume sediment
For each incubation, the methane oxidation rate per volume sediment slurry was determined via linear regression of the time points 1, 2, 3 and 4 (17 h, 42.5 h, 67 h and 142.5 h). The 95% confidence intervals were calculated. Rates per cm^3 wet sediment are 5x higher than for the sediment slurry (sediment + modified HEPES-buffered seawater), as displayed in Fig 1B (wet sediment = 20% of total slurry volume).

Quantification of absolute DIC concentrations via standard addition
For two incubations with sulfate, we quantified the absolute concentrations of DIC for the full time course of the incubations (Fig. S2B) using the standard addition method. 75 µl of each sample was mixed with 75 µl of a DIC standard (10.0 mM $NaHCO_3$) and analyzed for its isotopic enrichment ($^{13}F_{mix}(t_n)$). The absolute DIC-concentration of the sample ($[DIC](t_n)$, see Fig. S2B) was calculated as follows:

$$[DIC](t_n) = 10 \text{ mM} * (^{13}F_{mix}(t_n) - {}^{13}F_{std}) / (^{13}F(t_n) - {}^{13}F_{mix}(t_n))$$

Quantification of fractional abundance of $^{13}CH_4$ in the headspace used
The exact fraction of $^{13}CH_4$ (ca. 4.0 %) was quantified for individual incubations at the end of the 21 day incubation period via ^{1}H-NMR spectroscopy (Varian 400 MHz Spectrometer with broadband auto-tune OneProbe). Methane in the headspace was passed through chloroform-d (99.8% D, Cambridge Isotope laboratories) via a long 23G needle and acquired at 400 MHz with a repetition time of 10 s. Fractional abundances of ^{13}C in the methane were obtained via integration of the $^{12}CH_4$ signal and of the $^{13}CH_4$-satellites (iNMR version 4.3.0).

Quantification of residual sulfate
Residual sulfate was quantified via Ion chromatography on a DX-500 or DX-2000 instrument (Dionex, Sunnyvale, CA, USA) housed at the Caltech Environmental Analysis Center following the protocol outlined in (*33*). The DI water used throughout this study contained <10 µM residual sulfate. Incubations with 2,7-AQDS contained a maximum of 200 µM residual sulfate, from traces of sulfate present in the purchased material (176 µM per 10 mM 2,7-AQDS), which could not be removed via re-crystallization due to the high solubility of 2,7-AQDS (described in the chemicals and reagents section above). For all other incubations, the sulfate concentration remained below 50 µM throughout the incubation period.

Quantification of sulfide
Supernatant was removed via syringe and centrifuged in 0.6 ml eppendorf tubes (16000 rcf, 30 s). 20 µl of the clear supernatant was removed and added to 400 µl $Zn(OAc)_2$ (500 mM) to preserve the sulfide. Analysis was carried out in triplicate via the methylene blue method (*34*) using standards of 0.1, 0.25, 0.5, 1, 2, 5, 10 and 25 mM sulfide added to $Zn(OAc)_2$ (500 mM) in the same ratios as for the samples. Quantification was carried out in a plate reader (TECAN Sunrise^{TM}) by monitoring the absorbance at 670 nm.

Quantification of AQDS solubility in the incubation medium (data for Table S2)
Different regioisomers of AQDS (1,5-AQDS, 2,6-AQDS and 2,7-AQDS) were separately added to the modified artificial seawater described above, to a targeted final concentration of 25 mM. The suspensions were ultra-sonicated at room temperature to dissolve as much of the AQDS as possible. The tubes were kept at 4 °C or at 22.5 °C overnight. The tubes were centrifuged at 4 °C or 22.5 °C (16000 rcf, 30 min). The supernatant (300 µl) was mixed with 300 µl acetate (10.0 mM) as the internal standard and 100 µl deuterated water (99.9% D, Cambridge Isotope Laboratories) was added. The concentration of AQDS was obtained from integration of the ^{1}H-NMR spectra by comparison relative to the acetate standard.

Identity of reduced AQDS by UV-Vis and NMR
Reduced AQDS was identified photospectrometrically matching the spectra reported previously (*35*). Solutions containing reduced AQDS were paramagnetic (ca. 1000 Hz line width, ^{1}H-NMR spectroscopy), putatively due to the presence of the semiquinone-radical. Supernatant from an incubation that contained ca. 10 mM reduced AQDS was sparged with air for 30 min in order to re-oxidize AQH_2DS back to AQDS. ^{1}H-NMR spectroscopy shows full conversion to AQDS, undistinguishable from the AQDS used initially. No signals other than AQDS or HEPES buffer were visible in the spectrum, proving reversible reduction and oxidation without detectable formation of side products.

Quantification of reduced AQDS by iodometry
Reduced AQDS (2,6-AQH_2DS) was quantified via iodimetric titration in the anaerobic chamber. A standard solution of ca. 20 mM KI_3 was prepared as follows: iodine (254 mg, 2.0 mmol) and potassium iodide (1.66 g, 10 mmol) were dissolved in 100 ml DI water. After 2 days, the clear, dark solution was N_2-sparged and brought into the anaerobic chamber. The exact concentration of the KI_3 standard solution was quantified to be 19.5 mM via duplicate titration with sodium thiosulfate (exactly 101.5 mM, N_2-sparged). Procedure for the quantification of reduced AQDS in the incubations: 1000 µl anaerobic assay solution centrifuged in the anaerobic chamber + 200 µl anaerobic HEPES (1.0 M, pH = 7.5) + KI_3 standard solution as needed until color minimum, added in steps of 100 µl first, than in steps of 10 µl when closer to the equivalence point.

Control experiments without methane
Sediment incubations with AQDS (10 mM) under nitrogen did not generate substantial amounts of reduced AQDS (less than 1 mM after 3 weeks). To confirm that the methanotrophic microorganisms in the sediment had not been killed during the nitrogen +

AQDS incubation, methane was later injected into these incubation bottles after 3 weeks. Upon addition of methane, AQDS was reduced at rates similar to that shown in Fig. 1.

Check for methanogenic activity
Sediment slurries were incubated under a nitrogen headspace in duplicates without an added oxidant to probe for endogenous methanogenic activity. After 6 days, methane in the headspace was quantified via GC-MS (Hewlett Packard 5890 Series II gas chromatograph with mass selective detector 5972) by triplicate injections. For the first biological replicate, methane was found at a concentration that was close to the detection limit, corresponding to a specific methanogenesis rate of 0.5 ± 0.25 nmol methane (cm^3 wet sediment)$^{-1}$ d^{-1}. For the second replicate, the methane peak was too small for accurate quantification, but we can state an upper limit of 0.25 nmol (cm^3 wet sediment)$^{-1}$ d^{-1}. Based on these measurements, the endogenous methanogenesis rate [and/or enzymatic equilibration rate (*27, 28*) is ca. 3000x lower than methane oxidation with sulfate.

Thermodynamic calculations
The standard free energy for AOM with AQDS was calculated from the corresponding redox-potentials:
$HCO_3^- + 4\ H_2 + H^+ = CH_4 + 2\ H_2O \quad \Delta G°' = -135.3$ kJ mol^{-1}
$E°'$ for CH_4/HCO_3^- = -414 mV - $\Delta G°'/(nF)$ = -239 mV
$E°'$ for 2,6-AQDS = -186 mV [$E° = +228$ mV (*36*)]
$\Delta E°' = 53$ mV, $\Delta G°' = -nF\Delta E°' = -41$ kJ mol^{-1}

Methods for microbial anabolic activity measurements

Incubations for FISH-nanoSIMS and RNA analysis
For AOM incubations with sulfate or AQDS that were used for nanoSIMS (Fig. 3 and Fig. 4A) and RNA analysis (Fig. 2), incubations experiments were set up following the AOM-rate measurements described above (initially containing 1.0 mM ammonium without ^{15}N label). Methane oxidation rates were tracked in these incubations via the ^{13}C label. After 11 days, ca. 3.5 ml of supernatant remained in the serum bottles to which 3.0 ml artificial seawater without ammonium containing either 25 mM AQDS, 28 mM sulfate, or no oxidant was added. Next, 0.1 ml $^{15}NH_4^+$ (100 mM) was injected to yield about 2.0 mM ammonium with ca. 75% ^{15}N. Methane oxidation was monitored. After additional 8 days, the medium of the AQDS incubations was exchanged by 5.0 ml new medium containing 25 mM AQDS and 2.0 mM $^{15}NH_4^+$. Now the AQDS incubations contained ca. 95% $^{15}NH_4^+$ in the ammonium pool. The cultures were incubated for additional 10 days before harvest. Total incubation time with labeled ammonium: 18 days. Average labeling strength: ca. 75% for sulfate and no oxidant control; ca. 86% for the AQDS incubations.
For the second independent set of experiments with iron citrate, humic acids and sulfate (Fig. 4B), the medium contained 1.0 mM ammonium with ca. 40% ^{15}N label throughout the incubation period. These experiments were carried out from identical incubations that were for the AOM rate measurements (highlighted in Table S3).

Sampling for FISH-nanoSIMS and RNA

After 18 days incubation in the presence of $^{15}NH_4^+$, each incubation was shaken to suspend the sediment and 1.0 ml sediment slurry was sampled using a disposable sterile needle and syringe (ca. 0.3 ml wet sediment). The sediment aliquot was briefly centrifuged (4000 rcf) in an eppendorf tube and 0.5 ml of the supernatant was removed for DIC and metabolite analysis. 0.5 ml 4% paraformaldehyde in PBS (100 mM phosphate pH=7.4, salinity=10 g l^{-1}) was then added to the remaining 0.5 ml sediment slurry (2% formaldehyde final), resuspended and fixed for 120 min at 4 °C. The fixed sediment was subsequently washed 3 times with 1X PBS, followed by a single wash in EtOH/PBS (1:1) and then re-suspended in EtOH/PBS (1:1) to a final volume of 0.5 ml that was used for microscopy and nanoSIMS.

All remaining sediment from the identical incubations (ca. 0.7 ml wet sediment, see above) was removed for RNA analysis using a disposable sterile needle and syringe. The sediment slurry was immediately centrifuged (16000 rcf, 15 s), followed by removal of the supernatant and flash-freezing of the sediment pellet in liquid N_2. Frozen sediment was stored at -80 °C until RNA extraction.

RNA extraction, PCR, clone library construction, and phylogenetic analysis

RNA was extracted from the 0.7 ml frozen wet sediment described above using the RNA Powersoil Total RNA Isolation Kit (cat # 12866-25; MO BIO Laboratories, Inc., Carlsbad, CA, USA) with modifications (*37*). The eluted RNA was immediately DNase treated using the MO BIO RTS DNase Kit (cat no. 15200-50, MO BIO Laboratories, Inc., Carlsbad, CA, USA), purified and concentrated to 24 µl using the Qiagen RNeasy Plus Micro Kit (cat # 74034, Qiagen, Valencia, CA, USA), and converted to cDNA using the Invitrogen Superscript III First-Strand Synthesis SuperMix (cat no. 18080-400, ThermoFisher Scientific, Grand Island, NY, USA) with no reverse transcriptase (NRT) controls following manufacturer's instructions. cDNA was stored at -80 °C until further processing.

PCR conditions were as follows: 1 x 5 PRIME HotMasterMix buffer (cat # 2200400; 5 PRIME, Inc., Gaithersburg, MD, USA), 0.4 µM of each forward and reverse primer, and 1 µl of cDNA in a final volume of 25 µl. Methyl-coenzyme reductase alpha subunit (mcrA, primers ME1: GCMATGCARATHGGWATGTC /ME2 TCATKGCRTAGTTDGGRTAGT) and archaeal and bacterial 16S rRNA (primers Arc23F: TTCCGGTTGATCCYGCCGGA or Bac27F: AGAGTTTGATYMTGGCTC with U1492R: GGYTACCTTGTTACGACTT) were amplified with 40 cycles as described in (*38*). The cDNA from the sulfate microcosm was diluted 1/50 to have similar amount of amplicons compared with other cDNA samples. 5 µl of the PCR products was quantified in 1% (w/v) agarose electrophoresis with SYBR safe stain under ultraviolet light, and NRT controls did not show any amplification. The remainder of the PCR product for each sample was immediately cleaned by filtration (MultiScreen PCR Filter Plate #MSNU03010, Millipore) and resuspended to the original volumes using Tris–HCl (pH 8). 1 µl of the cleaned PCR product was used per ligation reaction and cloning according instructions in the TOPO TA Cloning Kit for Sequencing using the pCR4-TOPO Vector and One Shot Top 10 chemically competent *Escherichia coli* (Life Technologies). Recombinant clones were checked for inserts by PCR, gel electrophoresis and sequenced using primers M13F (5′-GTAAAACGACGGCCAG-3′) and M13R (5′-

CAGGAAACAGCTATGAC-3′) on an ABI Prism 3730 DNA sequencer using the BigDye Terminator v3.1 cycle sequencing kit (Applied Biosystems Inc., Foster City, CA, USA).
Sequences were manually checked and contigs assembled using the Sequencer v4.1.4 software. Sequences were then compared against the SILVA 16S rRNA database [version 119 (*39*)] or GenBank DNA database by using the BLAST algorithm (*40*). Alignment against reference sequences was completed using the SILVA online aligner (*39*) for 16S rRNA and ClustalO for mcrA, and aligned sequences were then imported into the ARB package version 6.0.2 (*41*) and manually verified. An additional 80 16S rRNA sequences were retrieved from SILVA database and 44 mcrA sequences were retrieved from NCBI Refseq and used as references for the phylogenetic analyses. The Bayesian phylogeny was generated using 1421 aligned 16S rRNA nucleic acid positions (inverse gamma rates) and 248 aligned mcrA amino acid positions (mixed amino acid model) using MrBayes v3.2.2 (*42*) until split frequencies were less than 0.01. Clone library sequences fall into several clades of high phylogenetic support. Clone library sequences fall into several groups of high phylogenetic support. One representative sequence is used to represent highly similar sequences; the number of sequences represented and the representative accession number are indicated in brackets in Figure 2. mcrA sequences were classified into groups as previously (*43*). Clone library sequences for archaeal 16S rRNA and mcrA genes, and bacterial 16S rRNA genes were deposited in NCBI under accession numbers KU324182 to KU324260, KU324346 to KU324428, and KU324261 to KU324345, respectively.

Illumina Tag sequencing (data for Fig. S4)
DNA was extracted from 0.25 g of wet weight sediment using the PowerSoil DNA Isolation Kit (Cat#12888-05, Mo Bio Laboratories, Carlsbad, CA). PCR amplification and barcoding of the 16S rRNA gene were performed as described previously (*44*). Amplicons for deep sequencing were outsourced to Laragen, Inc
(Culver City, CA) and run on an Illumina MiSeq platform (*44*). Data was analyzed using QIIME 1.8.0 (*45*) and processed sequences were assigned to phylotypes using a 99% similarity cutoff to the SILVA database version 115 (*39*) following previous procedures (*44*).

Sample preparation for aggregate embedding, sectioning, FISH, and nanoSIMS
Sample preparation was carried out following the recently optimized protocol in our lab outlined in (*8*). Briefly: Paraformaldehyde fixed consortia were detached from the sediment particles via sonication on ice with a sterile remote-tapered microtip probe (Branson) inserted into the liquid. Aggregates were concentrated on a 3 µm filter, covered in molten noble agar (2%) and embedded in glycol methacrylate (Heraeus Kulzer - Technovit® 8100). Sections of ca. 1 µm thickness were cut and stretched on a water droplet on a polylysine coated slide with teflon wells (Tekdon Inc) and analyzed by fluorescence *in situ* hybridization (FISH). Images of the FISH-stained consortia were collected and the location of these consortia were mapped for subsequent nanoSIMS analysis as described below.

FISH conditions and probes for this study
The FISH hybridization on thin sections of resin embedded microbial aggregates followed the recently optimized protocol described in (*8*). The phylogenetic identity of microorganisms in the thin sections were determined using conventional FISH using oligonucleotide probes fluorescently labeled on both the 5' and 3' ends (dual labeled) as outlined below. The FISH hybridization followed a standard protocol (*46*) and used a hybridization buffer containing 60% formamide and incubation at 46 °C for 120 min. Followed by a wash step at 48 ºC for 10 min. remove excess of probes. Visualization via epifluorescence microscopy (light source EXFO, X-Cite, Series 120 Q) was accomplished by mounting the hybridized sample with a mixture of DAPI-Citifuor (5 µg DAPI/ml) and imaging with a 100x objective (Microscope Olympus BX51, objective UPlan FL N, 100x /1.30 Oil, ∞/0.17/FN 26.5). The following FISH probes were used in this study (final concentration 2.5 ng/µl for each):
S-D-Arch-0915-a-A-20 in FITC, dual labeled: 5' to 3'= GTGCTCCCCCGCCAATTCCT (*47*)
S-*-ANME2c-0760-a-A-18 in Cy3, dual labeled: 5' to 3'= CGCCCCCAGCTTTCGTCC (*48*)
S-*-Dsb-0658-a-A-18 in Cy5, dual labeled: 5' to 3'= TCCACTTCCCTCTCCCAT (*49, 50*)

The overlay figures (Fig. 3 and Fig. S5-7) were contrast-adjusted for display purposes. FITC channel (Arc 915) is not shown. For aggregates that were positively stained for both, ANME-2c and for DSS, the DAPI channel was omitted for the overlay image.

nanoSIMS procedures and parameters for this study
After FISH and mapping (described above), the glass slides were scored and broken to size to fit in the Cameca "Geology" holder for the nanoSIMS, and coated with 50 nM gold to enhance conductivity. Secondary ion mass spectrometry analysis was carried out on a nanoSIMS 50L instrument (Cameca) using a primary Cs^+ ion beam. Pre- sputtering of target consortia was conducted with 100 pA current at D1=1 until 70,000-1,000,000 counts were reached on the ^{12}C detector. Analytical conditions included a 256x256 raster (or 512x512 raster for frames larger than 35 µm), ES=2, D1=4 (0.5 pA of current). Chained analyses were set up using SIBC, EOS, and HMR automatic peak centering every 2 frames using the $^{14}N^{12}C^-$ ion as reference. The following secondary ions were collected during the analysis: $^{12}C^-$, $^{13}C^-$, $^{12}C^{14}N^-$, $^{12}C^{15}N^-$, $^{32}S^-$, $^{33}S^-$ and $^{34}S^-$. 1-4 frames were collected for each aggregate. The ions $^{12}C^{14}N^-$ and $^{12}C^{15}N^-$ were used for the fractional abundances of ^{15}N reported in this study.

nanoSIMS data processing
Raw nanoSIMS data files were initially processed in the Matlab-based program Look@NanoSIMS (*51*) to align and accumulate frames and extract ion count data. FISH images of aggregates (described above) were used to define regions of interest (ROIs) on the nanoSIMS ion images that correspond to archaeal or bacterial biomass. Total ion counts in each ROI for $^{12}C^{15}N^-$ and $^{12}C^{14}N^-$ were used to calculate partner-specific relative biosynthetic activity ($^{15}N/(^{14}N+^{15}N)$) for each aggregate (data for Fig. 4A and 4B). For display purposes the median image filter medfilt2 from the Matlab Image

Processing Toolbox was applied to the images of aggregate fractional abundance ^{15}N to reduce the noise of abnormally bright pixels. This filter was not applied to the raw data for any analyses.

Calculation of doubling times from average cellular ^{15}N after 18 days ($^{15}F_{18days}$)

Fraction of new biomass: $x = [B_{18days}-B_0] /B_{18days}$

With exponential growth: $x = 1 - \exp(-\mu * 18 \text{ days})$

With $^{15}F_0 \approx 0$: $^{15}F_{18days} = x * {}^{15}F_{NH4+}$

Specific growth rate: $\mu = -\ln(1-{}^{15}F_{18days} / {}^{15}F_{NH4+})/18 \text{ days}$

Doubling time: $t_d = \ln(2)/\mu$

$^{15}F_{NH4+} = 0.75$ for sulfate and 0.86 for AQDS (see "Incubations for FISH-nanoSIMS")

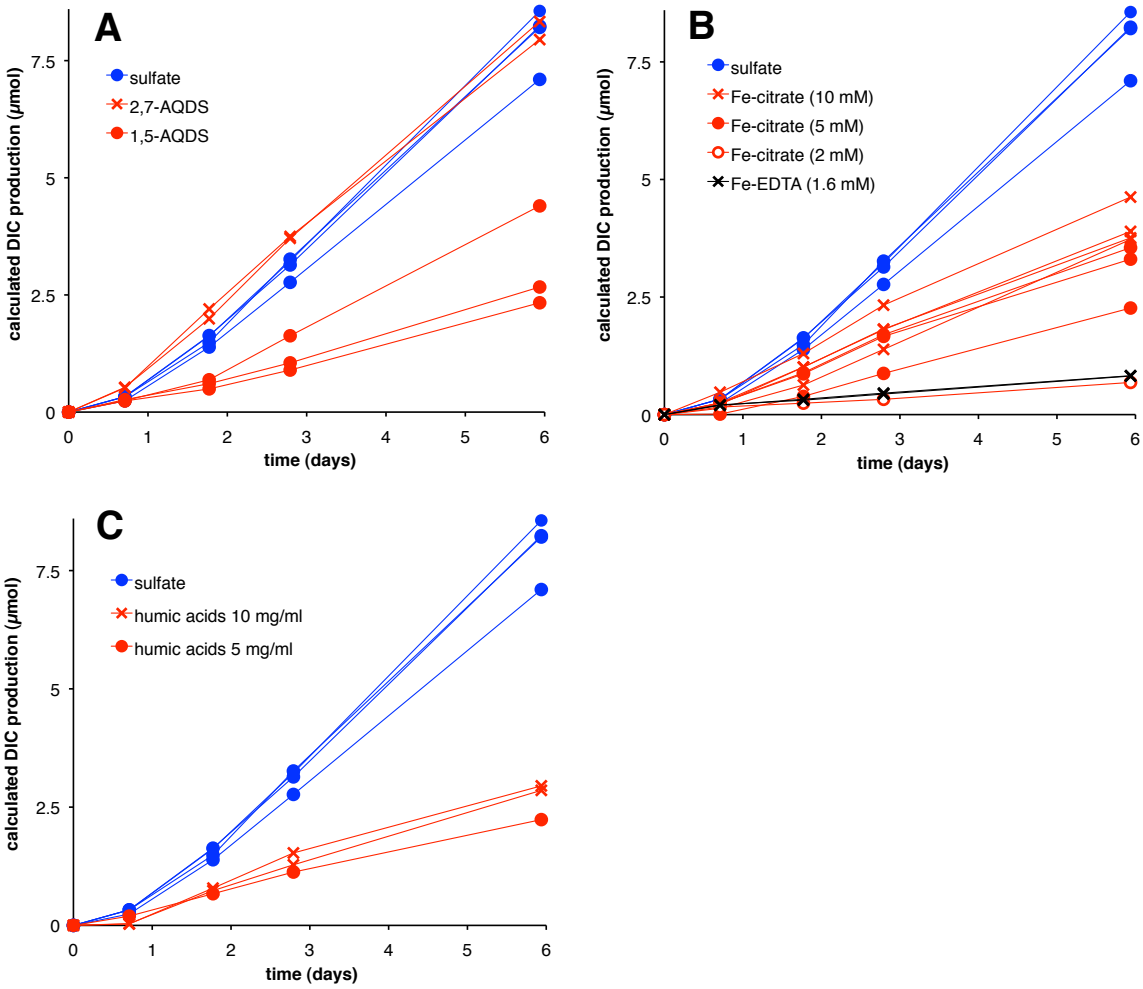

Fig. S1: AOM with different oxidants. Time courses for rates described in Fig. 1B (red curves); AOM rates with sulfate are included as a reference (blue curves, representing identical data as shown in Fig. 1A).

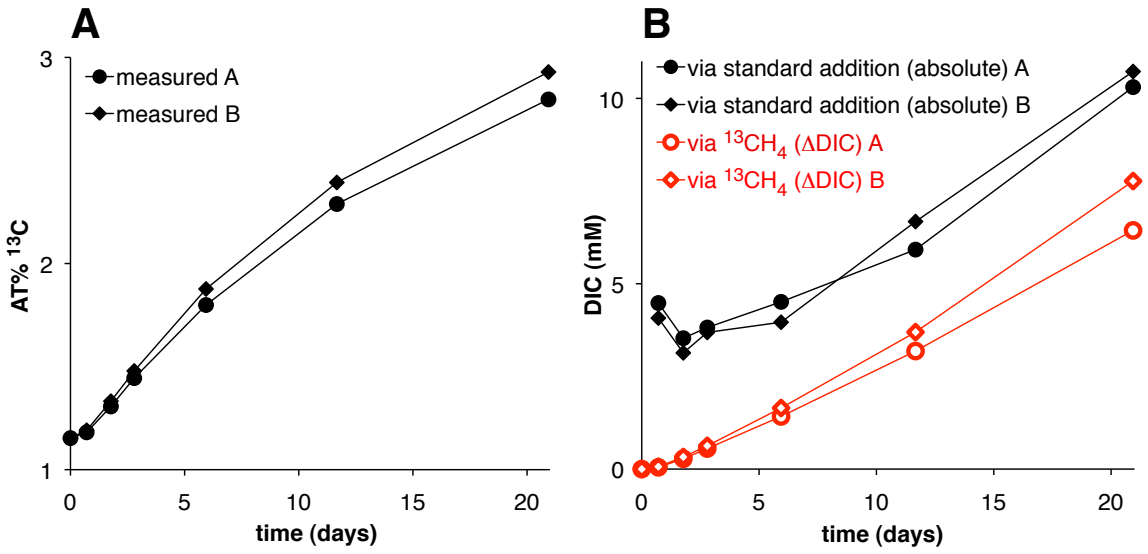

Fig. S2: Comparison of raw data and calculated concentrations of DIC. Data for two replicate incubations with sulfate-coupled AOM (Table S3, incubations "Sulfate [28 mM] A+B") that are used for Fig. 1A and Table S1B are shown as examples. **A**: Time course of AT% ^{13}C measured in DIC. **B**: Calculated concentrations of total (black) and newly formed (red) DIC (see methods). **Red**: Calculation used throughout this publication that yields the concentration of newly formed DIC. This method relies on knowing the AT% ^{13}C in the methane employed and the initial concentration and isotopic composition of DIC. **Black:** Independent method via standard addition that directly yields the absolute concentration of DIC for any time point. We employed this method to provide evidence for net DIC increase during incubations. This method does not account for the inorganic carbon present as gaseous CO_2 in the headspace.

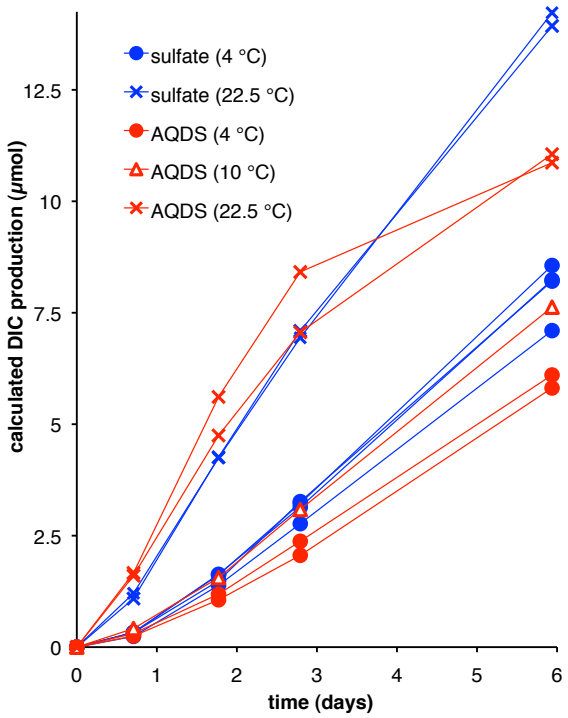

Fig. S3: Time course of AOM with sulfate and AQDS at 22.5 °C. Data from experiments at 4 °C included as a reference (• symbol, identical data as in Fig. 1A).

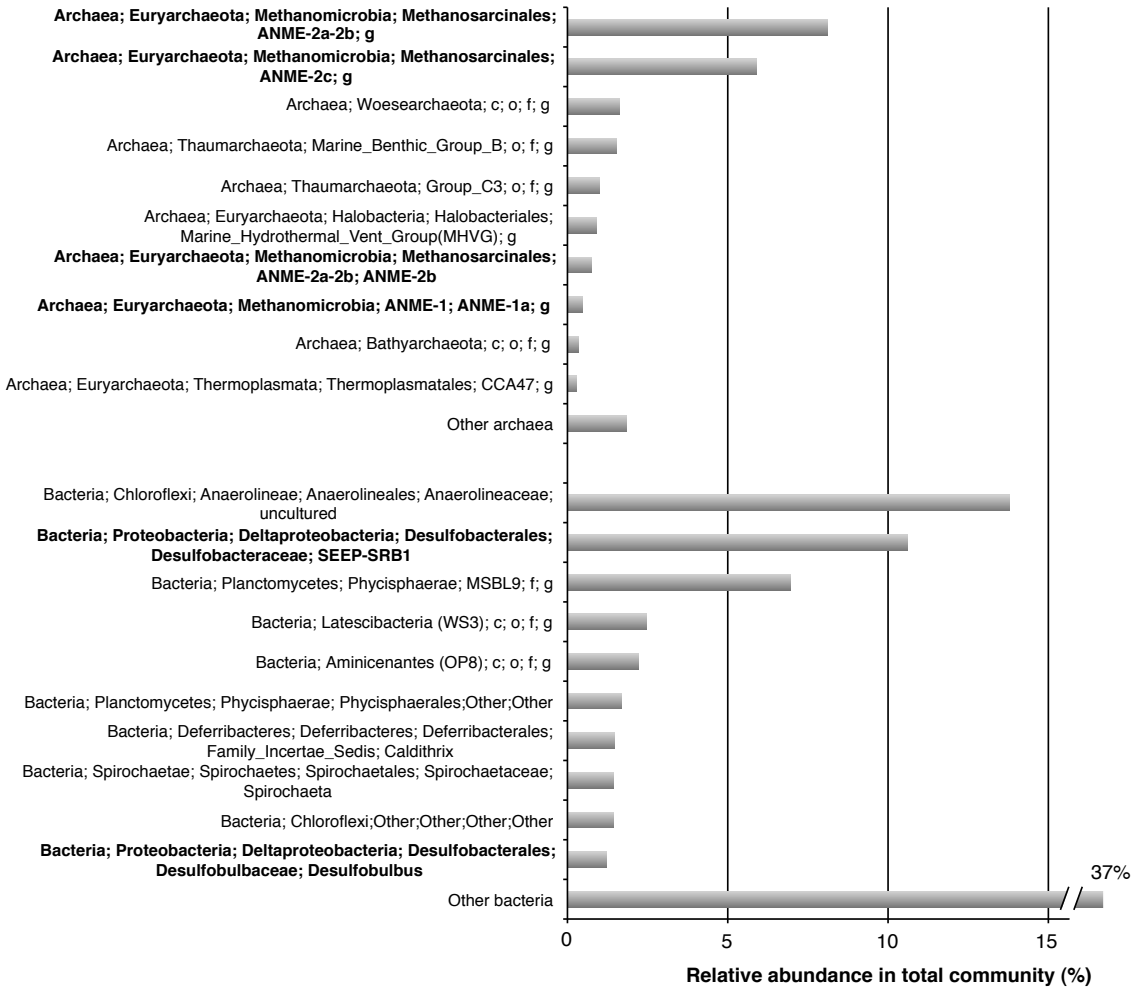

Fig. S4: Top 10 most abundant archaeal and bacterial genera in PC61. 16S rRNA gene Illumina TAG sequencing of the microbial assemblage in the initial PC61 sediment used for the microcosm experiments. Sequences were classified using the SILVA database release 119.

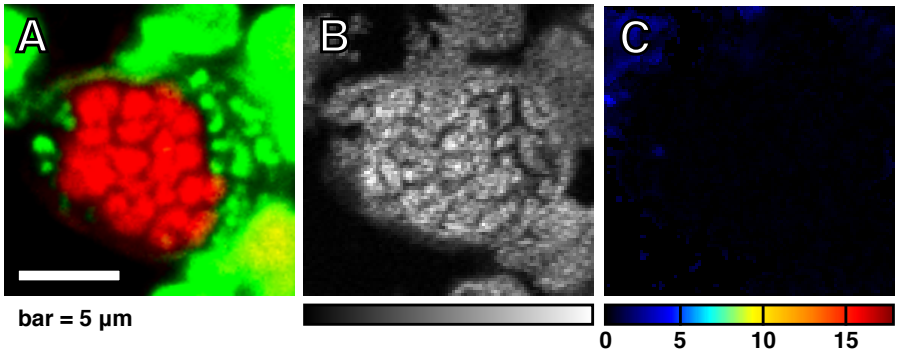

Fig. S5: Example FISH-nanoSIMS of consortium incubated without an oxidant. ANME-2c/ DSS consortium recovered from the microcosm treatment supplied with a methane headspace but no added electron acceptor. Data was acquired after 18 days of incubation in the presence of $^{15}NH_4^+$ (see Fig. 3A, inset). Panel **A**: FISH images, ANME-2c (in red), Desulfobacteraceae (in green). Panel **B**: nanoSIMS ion image of $^{12}C^{14}N^-$ showing cell biomass, linear scale. Panel **C**: fractional abundance of ^{15}N (in AT%) as a proxy for newly synthesized biomass.

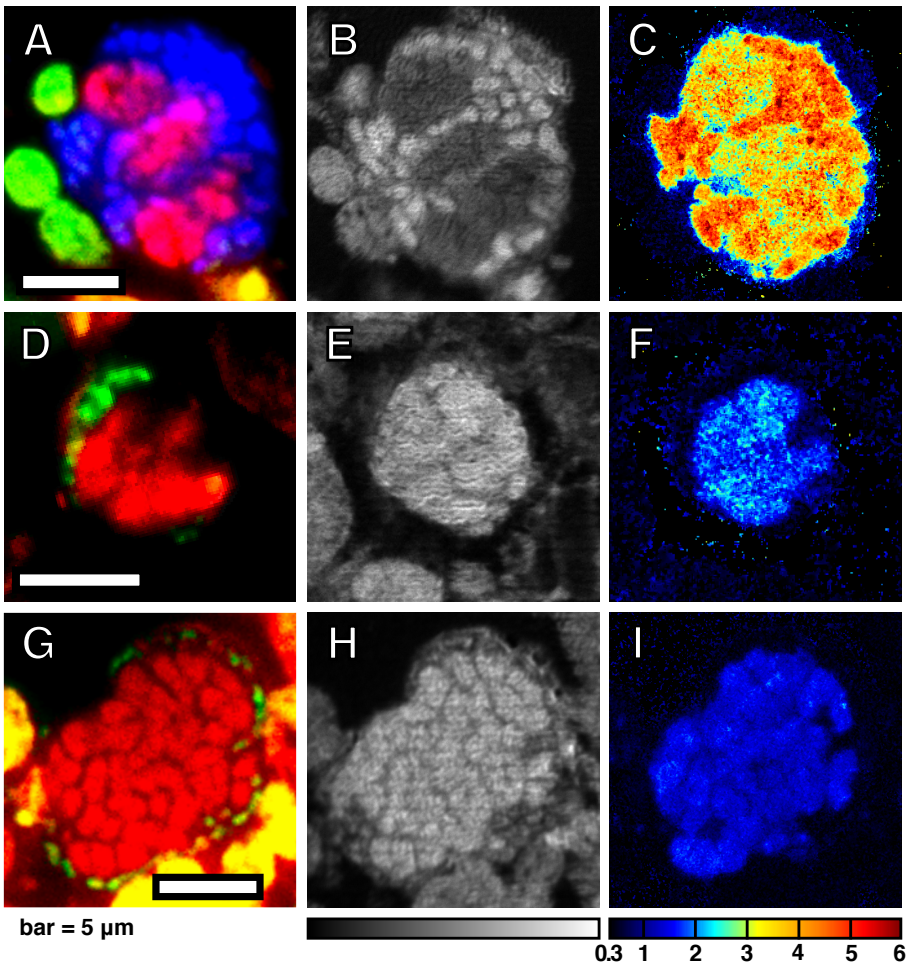

Fig. S6: FISH-nanoSIMS analysis of consortia incubated with different oxidants. Representative consortia recovered from a second set of experiments with PC61 (see Fig. 4B) incubated with ferric citrate, humic acids, or sulfate. Panels **A-C**: with sulfate; Panels **D-F**: with ferric citrate in the presence of the sulfate-reducing inhibitor sodium molybdate (25 mM); Panels **G-I**: with humic acids as the oxidant. Panels **A** & **D** & **G**: FISH images, ANME-2c (in red), Desulfobacteraceae (in green); for panel A DAPI image (in blue) included. Scale bar = 5 µm for all FISH images. Panels **B** & **E** & **H**: nanoSIMS ion image of $^{12}C^{14}N^-$ showing cell biomass, linear scale. Panel **C** & **F** & **I**: fractional abundance of ^{15}N (in AT%) measured by nanoSIMS as a proxy for newly synthesized biomass. Here, the minimum value on the scale was set to 0.3 AT% (black), close to the natural abundance ^{15}N (0.36 AT%).

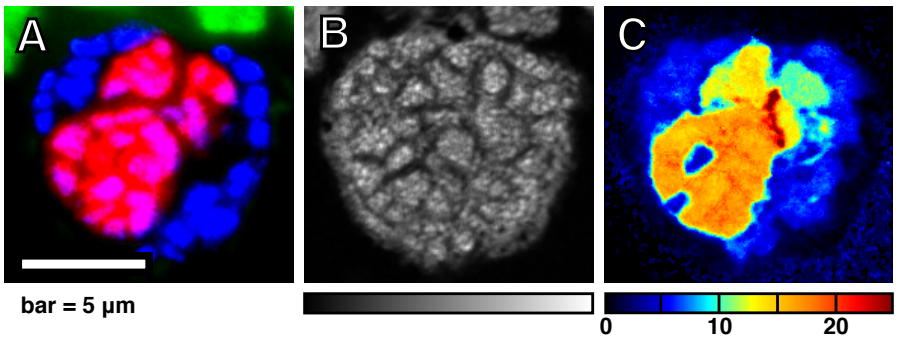

Fig. S7: FISH-nanoSIMS data from the outlier ANME-2c consortium. This consortium was excluded from the activity correlation (see Fig. 4A).* Panel **A**: FISH images, ANME-2c (in red), Desulfobacteraceae, DSS (in green), DAPI (in blue). Panel **B**: nanoSIMS ion image of $^{12}C^{14}N^-$ showing cell biomass, linear scale. Panel **C**: fractional abundance of ^{15}N (in AT%) as a proxy for newly synthesized biomass.

* The low ratio of bacterial/archaeal ^{15}N incorporation (ratio = 0.386) for incubations with sulfate is represents an outlier from all other analyzed consortia from this treatment as well as our previously published FISH-nanoSIMS experiments. For this reason, we excluded this ANME-2c aggregate (with an unidentified bacterial partner) from the linear regression of the overall activities displayed in Fig. 4A.

Table S1: Final concentration of reduced electron acceptors AQH_2DS and sulfide. Concentrations measured after a 21 day incubation (experiments in Fig. 1A) and calculated stoichiometry per DIC formed from methane.

A) Final concentrations of reduced AQDS (AQH_2DS):

Experiment	DIC formed [mM]	AQH_2DS [mM]	Stoichiometry*
AQDS 10 mM	2.39	8.6	3.60
AQDS 10 mM	2.64	9.6	3.62
AQDS 10 mM + MoO_4^{2-} 25 mM	2.82	9.8	3.45
AQDS 10 mM + MoO_4^{2-} 25 mM	2.59	9.2	3.55

* The lower amount of AQH_2DS found than expected (4:1 stoichiometry) may be attributed to partial oxidation during the process of sampling and titration.

B) Final concentrations of sulfide:

Experiment	DIC formed [mM]	sulfide [mM]*	Stoichiometry†
Sulfate 28 mM (A)	6.44	5.9	0.92
Sulfate 28 mM (B)	7.77	6.5	0.84
Sulfate 28 mM (C)	7.51	7.0	0.93
Sulfate 28 mM (D)	7.29	6.1	0.84

* sulfide [mM] = sum of HS^- and H_2S.

† The lower amount of aqueous sulfide measured relative to the expected 1:1 stoichiometry may be attributed to a combination of factors resulting in a loss of sulfide. These include some sulfide partitioning into the headspace as gaseous H_2S and possibly escaping as gaseous H_2S during sampling, partial sulfide oxidization during the sampling and centrifugation on the benchtop, or possibly precipitation with divalent cations during the incubation.

Table S2: Solubility of different AQDS regioisomers in the incubation medium.

Compound	4 °C	22.5 °C
2,6-AQDS (AQDS)	0.9 mM	1.9 mM
2,7-AQDS	>25 mM	>25 mM
1,5-AQDS	2.5 mM	not determined

Table S3: List of all oxidants tested for AOM. The percentage AOM rates are reported relative to sulfate-coupled AOM (1.50 µmol cm^{-3} day^{-1}). **Top**: Summary of compounds described in Fig. 1B; **Bottom**: Oxidants resulting in an AOM rate less than 0.10 µmol cm^{-3} day^{-1} (< 7% rel. to sulfate as oxidant).

Oxidant [conc.], replicates	E°' (mV)	Addition of 25 mM MoO_4^{2-}	Rate relative to AOM with sulfate (%)
Sulfate [28 mM] A,B,C*,D	-220	−	100
Sulfate [28 mM] E,F,G		+	20
AQDS [10 mM] A,B	-186 (*36*)	−	74
AQDS [10 mM] C,D		+	83
No oxidant A,B		−	1.5 †
No oxidant + H_2CO (4%) A,B		−	0
2,7-AQDS [10 mM] A,B	-185 (*36*)	−	97
1,5-AQDS [10 mM] A,B,C	-175 (*36*)	−	38
Fe(III)-citrate [10 mM] A	372 (*52*)	−	53
Fe(III)-citrate [10 mM] B*,C,D		+	46
Fe(III)-citrate [5 mM] A,B,C		+	37
Fe(III)-citrate [2 mM]		+	7
Fe(III)-EDTA [1.6 mM] A,B	96 (*53*)	−	8
Humic acids [1%] A*,B	n.a.‡	−	36
Humic acids [0.5%]		−	26
Melanin [8 mg/ml]	n.a.‡	+	6.4 §
Melanin [2 mg/ml]		+	4.3
Melanin [0.5 mg/ml]		+	2.6
Fe(III)-citrate [25 mM]	372 (*52*)	+	2.5
Fe(III)-NTA [1 mM]		−	2.5
Fe(III)-NTA [10 mM]	385 (*52*)	−	≤ 1.5 †
Fe(III)-EDTA [10 mM] A,B	96 (*53*)	−	≤ 1.5 †
Phenazine methosulfate [1 mM]	80 (*54*)	−	≤ 1.5 †
Methylene blue [1 mM]	11 (*54*)	−	≤ 1.5 †
Indigo tetrasulfonate [10 mM; 1 mM]	-46 (*54*)	−	≤ 1.5 †
Resazurin [10 mM]	-51 (*55*)	−	≤ 1.5 †
1-Hydroxynaphthoquinone [10 mM; 1 mM]	-137 (*54*)	−	≤ 1.5 †
Phenosafranine [10 mM; 1.6 mM]	-252 (*54*)	−	≤ 1.5 †
Safranine T [10 mM; 1.6 mM]	-289 (*54*)	−	≤ 1.5 †

* Replicate that was analyzed via nanoSIMS (see Fig. 4B and Fig. S6).

† No net methane oxidation can be deduced, because incubations without oxidant show an apparent AOM rate of 0.023 µmol cm^{-3} day^{-1} (1.5% relative to sulfate). This label conversion of $^{13}CH_4$ to ^{13}C-DIC arises via enzyme catalyzed isotope exchange between $^{13}CH_4$ and DIC without net methane oxidation [(*27, 28*), also discussed in main part and in the methods section].

‡ The midpoint reduction potentials of humic acids and melanin are not well defined. Both compounds can act as single electron acceptors due to their quinone moieties as shown experimentally for humic acids (*56*) and for melanin (*57*). The melanin used was a gift from Kenneth Nealson (University of Southern California) that is kindly acknowledged.

§ AOM occurs linearly, rates per wet sediment: with 8 mg/ml melanin: 0.096 ± 0.020 µmol cm^{-3} day^{-1}; with 2 mg/ml melanin: 0.064 ± 0.012 µmol cm^{-3} day^{-1}; with 0.5 mg/ml melanin: 0.039 ± 0.015 µmol cm^{-3} day^{-1}.

Table S4: Bacterial 16S rRNA diversity. Recovered from AOM microcosms supplied with sulfate, AQDS, or no added oxidant.

Bacterial 16S cDNA sequences recovered*	Oxidant		
	Sulfate	AQDS†	none
Proteobacteria/Deltaproteobacteria/Desulfobacterales_Desulfobacteraceae/SEEP-SRB1	**18**	**2**	**0**
Proteobacteria/Deltaproteobacteria/Desulfuromonadales/Desulfuromonadaceae_Pelobacter_2	2	3	0
Bacteroidetes/Sphingobacteriia_Sphingobacteriales_1/WCHB1-69	2	0	0
Chlorobi/Ignavibacteria_Ignavibacteriales/BSV26	2	0	0
Proteobacteria/Deltaproteobacteria/Desulfarculales_Desulfarculaceae/uncultured	2	0	0
Proteobacteria/Gammaproteobacteria_1/Pseudomonadales_Pseudomonadaceae/Pseudomonas_1	1	3	0
Chloroflexi/Anaerolineae_Anaerolineales_Anaerolineaceae/uncultured	1	1	1
Proteobacteria/Deltaproteobacteria/Sva0485	1	1	0
Acidobacteria/Subgroup 22	1	0	0
Candidate division OP8	1	0	1
Proteobacteria/Deltaproteobacteria/Sh765B-TzT-29	1	0	0
Proteobacteria_Deltaproteobacteria_Desulfobacterales_Nitrospinaceae/uncultured	1	0	0
Spirochaetae_Spirochaetes/Spirochaetales/Spirochaetaceae/Spirochaeta_2	0	9	1
Proteobacteria/Betaproteobacteria/Burkholderiales/Oxalobacteraceae/Herbaspirillum_1	0	4	0
Candidate division JS1	0	2	3
Proteobacteria/Epsilonproteobacteria/Campylobacterales_Helicobacteraceae/Sulfurimonas	0	2	1
Bacteroidetes/Flavobacteriia_Flavobacteriales/Flavobacteriaceae_1/Maritimimonas	0	1	0
Chloroflexi/Ardenticatenia/uncultured	0	1	1
Firmicutes_Clostridia_1/Clostridiales/Family XII/Fusibacter	0	1	0
Proteobacteria/Alphaproteobacteria/Rhizobiales_1/Brucellaceae/Ochrobactrum_1	0	1	0
Actinobacteria/Acidimicrobiia_Acidimicrobiales/OM1 clade	0	0	3
Bacteroidetes/BD2-2	0	0	2
Bacteroidetes/Bacteroidia_Bacteroidales/Porphyromonadaceae_4/uncultured	0	0	1
Candidate division WS3	0	0	1
Chloroflexi/Dehalococcoidia/GIF9	0	0	1
Lentisphaerae/B01R017	0	0	1
Planctomycetes/Phycisphaerae/MSBL9	0	0	1
Planctomycetes/Phycisphaerae/Phycisphaerales/AKAU3564 sediment group	0	0	1
Proteobacteria/Gammaproteobacteria_2/Chromatiales_Ectothiorhodospiraceae_Acidiferrobacter	0	0	1
Spirochaetae_Spirochaetes/Spirochaetales/Leptospiraceae/uncultured	0	0	1
TOTAL NUM OF CLONES	**33**	**31**	**21**

* Data based on 16S cDNA clone libraries.
† PCR amplification and cloning of bacterial cDNA from the AQDS treatment was challenging due to weak amplification, few insert containing clones, and chimeric sequences.

Table S5: nanoSIMS ^{15}N and ^{14}N total ion counts. Calculation of ^{15}N fractional abundance (anabolic activity proxy) for paired archaea (a) and bacteria (b) in consortia from all 6 incubation conditions supplied with $^{15}NH_4^+$.

no	ANME	a ^{14}N counts	a ^{15}N counts	b ^{14}N counts	b ^{15}N counts	a ^{15}N fraction	b ^{15}N fraction
Set 1: Sulfate							
1	2c	8186903	910346	4986312	770403	0.1001	0.1338
2*	2c	13234012	2228293	9988379	591393	0.1441	0.0559
3	2c	1017392	100206	4734445	514724	0.0897	0.0981
4	other	10447750	1350011	16572950	2779724	0.1144	0.1436
5	2c	2896866	327406	4306194	530991	0.1015	0.1098
6	other	5173791	509800	10152972	1060263	0.0897	0.0946
7	2c	8069719	1053146	10253054	1436464	0.1154	0.1229
8	other	9548875	1646186	11052811	2226646	0.1470	0.1677
9	2c	15412698	1470548	7454752	836300	0.0871	0.1009
10	other	1254227	172559	434489	81620	0.1209	0.1581
11	other	523351	45850	455947	57855	0.0806	0.1126
12	2c	586645	57716	467545	63416	0.0896	0.1194
13	2c	9284639	274089	992128	22318	0.0287	0.0220
14	other	13355485	2529941	10646441	2223613	0.1593	0.1728
15	2c	8150920	509359	7548831	1069396	0.0588	0.1241
16	2c	9090606	1285688	3806417	560889	0.1239	0.1284
17	2c	4446504	383623	2105270	223125	0.0794	0.0958
18	other	6543141	886483	4962457	687646	0.1193	0.1217
19	other	5192683	506817	3032520	326993	0.0889	0.0973
20	other	4772514	558378	5406186	765379	0.1047	0.1240
Set 1: AQDS							
1	2c	6072396	126268	3174807	14796	0.0204	0.0046
2	2c	6738562	291479	2337765	15076	0.0415	0.0064
3	2c	4174136	678303	6944724	45479	0.1398	0.0065
4	2c	4421657	39358	3701860	21362	0.0088	0.0057
5	2c	9024087	1521364	2290624	45313	0.1443	0.0194
6	other	12497523	3481819	1829789	34577	0.2179	0.0185
7	other	14933629	1359298	5258297	43004	0.0834	0.0081
8	other	34700825	3797466	14097837	164882	0.0986	0.0116
9	2c	1400937	5689	1219111	5187	0.0040	0.0042
10	other	4102974	1339454	656114	19576	0.2461	0.0290
11	2c	1932351	87738	2609306	17195	0.0434	0.0065
12	2c	5872808	85174	11129659	48086	0.0143	0.0043

13	2c	21909385	1429092	16271732	172963	0.0612	0.0105
14	2c	25267632	301796	14219942	66618	0.0118	0.0047
15	other	5632270	1292904	2895095	27853	0.1867	0.0095
16	other	27058715	4864118	7520936	135132	0.1524	0.0177
17	other	18133896	4135568	10299199	145195	0.1857	0.0139
18	other	23419015	5468125	7276084	112843	0.1893	0.0153
19	2c	29832362	2586694	10923964	142677	0.0798	0.0129

Set 1: no oxidant

1	other	27743268	116427	26164833	108451	0.0042	0.0041
2	other	10368296	44295	5406673	22582	0.0043	0.0042
3	2c	5725992	23424	2571274	10786	0.0041	0.0042
4	2c	2337391	9594	1496614	6431	0.0041	0.0043
5	2c	4006009	16847	2432421	10715	0.0042	0.0044
6	2c	796822	3103	637887	3373	0.0039	0.0053
7	other	2168580	9002	913893	3964	0.0041	0.0043
8	other	2027340	8569	533112	2280	0.0042	0.0043
9	2c	594977	2510	250708	1120	0.0042	0.0044

Set 2: Sulfate

1	2c	8087694	305021	9201606	439261	0.0363	0.0456
2	2c	14667860	628799	5998433	346787	0.0411	0.0547
3	2c	15123316	455273	15751906	646736	0.0292	0.0394
4	2c	6143931	236920	5971520	312392	0.0371	0.0497
5	other	6096641	123600	5619590	142946	0.0199	0.0248
6	other	910494	32272	655354	43321	0.0342	0.0620
7	2c	4214918	158386	9693657	426387	0.0362	0.0421
8	other	33488023	1268969	15216001	658815	0.0365	0.0415
9	2c	11309440	214881	7779576	280883	0.0186	0.0348
10	other	15482854	594463	5301457	275310	0.0370	0.0494
11	other	1786420	91861	1233988	92978	0.0489	0.0701
12	2c	9145651	409931	3955885	244739	0.0429	0.0583
13	2c	3867661	107011	1599231	69821	0.0269	0.0418
14	other	50990162	2917348	27076729	2189768	0.0541	0.0748
15	other	8328778	405356	7942316	478070	0.0464	0.0568
16	2c	36187900	1123734	15598271	783987	0.0301	0.0479
17	other	118836163	3398649	24451232	1322277	0.0278	0.0513
18	other	12972873	507426	16102047	823092	0.0376	0.0486
19	other	14351082	718547	5907655	372495	0.0477	0.0593

Set 2: Fe^{III}-citrate

1	other	13958433	256405	2142551	15908	0.0180	0.0074
2	2c	80658680	426938	40755590	159073	0.0053	0.0039
3	2c	7945594	76309	2466373	10663	0.0095	0.0043
4	2c	25346261	103012	30689462	121272	0.0040	0.0039
5	2c	24940312	115912	9047431	35106	0.0046	0.0039
6	2c	28445673	128781	7571431	30020	0.0045	0.0039
7	2c	17070092	79021	10395414	42311	0.0046	0.0041
8	2c	33377158	145571	26132592	108667	0.0043	0.0041
9	other	11158319	82807	4238780	18974	0.0074	0.0045
10	2c	90768537	415556	32521432	111492	0.0046	0.0034
11	other	5730271	84783	4685776	29842	0.0146	0.0063
12	other	1771637	9949	734437	3142	0.0056	0.0043
13	2c	1079883	7359	672707	2715	0.0068	0.0040
14	2c	13358256	63664	5039684	20964	0.0047	0.0041
15	2c	521199	5641	421875	2195	0.0107	0.0052
16	other	12034615	487803	4495900	97325	0.0390	0.0212
17	other	67354991	648685	23031378	98321	0.0095	0.0043
18	2c	26683636	137727	18050449	76041	0.0051	0.0042
19	other	34660589	858122	5156201	30589	0.0242	0.0059
20	2c	2726245	10646	1167407	4668	0.0039	0.0040
21	other	12633567	103769	3697589	23008	0.0081	0.0062
22	2c	1582971	9352	741502	3509	0.0059	0.0047
23	other	80592797	1264580	47868634	266877	0.0154	0.0055
24	other	7272802	197358	1815950	22945	0.0264	0.0125
25	2c	726949	3227	869859	3359	0.0044	0.0038
26	other	10556506	59782	2868653	11472	0.0056	0.0040
27	2c	3799183	66454	753031	4718	0.0172	0.0062
28	2c	249351	8235	159039	1582	0.0320	0.0098
29	2c	17565368	858385	8662755	94449	0.0466	0.0108
30	2c	4004142	16716	1971058	7616	0.0042	0.0038
31	2c	26175206	229809	10609375	36439	0.0087	0.0034

Set 2: Humic acids

1	other	55117751	205562	33614478	126802	0.0037	0.0038
2	2c	25490787	110116	16573079	62509	0.0043	0.0038
3	2c	16355923	62061	11353534	42632	0.0038	0.0037
4	2c	1714610	7232	2068626	7368	0.0042	0.0035
5	2c	15484727	68166	7298135	23485	0.0044	0.0032
6	other	27861590	191027	5821760	25592	0.0068	0.0044
7	other	21308772	78013	9206680	33601	0.0036	0.0036
8	2c	5096678	18894	1266090	4568	0.0037	0.0036

9	other	51484560	184292	30993892	110596	0.0036	0.0036
10	other	60947497	220325	28581153	101978	0.0036	0.0036
11	2c	8698946	32672	7242871	26593	0.0037	0.0037
12	2c	1706409	6586	4794201	17402	0.0038	0.0036
13	other	25317446	96727	7293172	27065	0.0038	0.0037
14	2c	3012438	65659	1078289	5336	0.0213	0.0049
15	2c	1589700	17382	132418	727	0.0108	0.0055
16	2c	2982865	10376	2787514	9735	0.0035	0.0035
17	other	12071094	204435	3823404	35601	0.0167	0.0092
18	2c	62533691	257650	29351492	116502	0.0041	0.0040
19	other	4661401	18127	3330721	12872	0.0039	0.0038
20	2c	1411693	5478	994683	3947	0.0039	0.0040
21	2c	12452346	48188	10019896	37442	0.0039	0.0037
22	2c	2756054	13427	2934052	11289	0.0048	0.0038
23	other	2230184	10036	1424952	5890	0.0045	0.0041
24	other	25175520	113101	9529710	38242	0.0045	0.0040
25	other	46314144	230182	13121757	51152	0.0049	0.0039
26	other	30810467	118178	21636937	80911	0.0038	0.0037
27	other	25912507	101075	25529653	95841	0.0039	0.0037
28	2c	6613731	27686	1335995	5250	0.0042	0.0039
29	2c	2821470	10703	494632	1923	0.0038	0.0039
30	2c	32229781	121891	12349381	46419	0.0038	0.0037
31	2c	29021850	128491	15403182	64994	0.0044	0.0042
32	2c	13268313	51047	3640947	13699	0.0038	0.0037
33	2c	3919208	24209	942992	3784	0.0061	0.0040
34	other	4830697	20192	1996265	7515	0.0042	0.0038
35	2c	105728195	1376562	16280903	106545	0.0129	0.0065
36	other	27989361	109408	20585970	78464	0.0039	0.0038
37	other	35846128	139036	5793441	22969	0.0039	0.0039
38	other	21421209	82112	23012457	86891	0.0038	0.0038
39	other	48875263	168401	54750403	186101	0.0034	0.0034
40	other	49043583	188027	6873982	25469	0.0038	0.0037
41	2c	2307701	8846	630923	2289	0.0038	0.0036
42	other	40320950	154632	18812307	71445	0.0038	0.0038
43	2c	20353901	81696	9496510	36161	0.0040	0.0038
44	2c	72837724	316207	27141409	82236	0.0043	0.0030
45	other	18002993	66271	8274426	30362	0.0037	0.0037
46	2c	17935549	70220	10335920	40134	0.0039	0.0039

*This aggregate was classified as outlier in Fig 4A (see also Fig. S7).

REFERENCES AND NOTES

1. A. Boetius, K. Ravenschlag, C. J. Schubert, D. Rickert, F. Widdel, A. Gieseke, R. Amann, B. B. Jørgensen, U. Witte, O. Pfannkuche, A marine microbial consortium apparently mediating anaerobic oxidation of methane. *Nature* **407**, 623–626 (2000). Medline doi:10.1038/35036572

2. V. J. Orphan, C. H. House, K. U. Hinrichs, K. D. McKeegan, E. F. DeLong, Methane-consuming archaea revealed by directly coupled isotopic and phylogenetic analysis. *Science* **293**, 484–487 (2001). Medline doi:10.1126/science.1061338

3. S. J. Hallam, N. Putnam, C. M. Preston, J. C. Detter, D. Rokhsar, P. M. Richardson, E. F. DeLong, Reverse methanogenesis: Testing the hypothesis with environmental genomics. *Science* **305**, 1457–1462 (2004). Medline doi:10.1126/science.1100025

4. S. Scheller, M. Goenrich, R. Boecher, R. K. Thauer, B. Jaun, The key nickel enzyme of methanogenesis catalyses the anaerobic oxidation of methane. *Nature* **465**, 606–608 (2010). Medline doi:10.1038/nature09015

5. M. F. Haroon, S. Hu, Y. Shi, M. Imelfort, J. Keller, P. Hugenholtz, Z. Yuan, G. W. Tyson, Anaerobic oxidation of methane coupled to nitrate reduction in a novel archaeal lineage. *Nature* **500**, 567–570 (2013). Medline doi:10.1038/nature12375

6. E. J. Beal, C. H. House, V. J. Orphan, Manganese- and iron-dependent marine methane oxidation. *Science* **325**, 184–187 (2009). Medline

7. J. Milucka, T. G. Ferdelman, L. Polerecky, D. Franzke, G. Wegener, M. Schmid, I. Lieberwirth, M. Wagner, F. Widdel, M. M. Kuypers, Zero-valent sulphur is a key intermediate in marine methane oxidation. *Nature* **491**, 541–546 (2012). Medline doi:10.1038/nature11656

8. S. E. McGlynn, G. L. Chadwick, C. P. Kempes, V. J. Orphan, Single cell activity reveals direct electron transfer in methanotrophic consortia. *Nature* **526**, 531–535 (2015). Medline doi:10.1038/nature15512

9. G. Wegener, V. Krukenberg, D. Riedel, H. E. Tegetmeyer, A. Boetius, Intercellular wiring enables electron transfer between methanotrophic archaea and bacteria. *Nature* **526**, 587–590 (2015). Medline doi:10.1038/nature15733

10. W. S. Reeburgh, Oceanic methane biogeochemistry. *Chem. Rev.* **107**, 486–513 (2007). Medline doi:10.1021/cr050362v

11. K. Knittel, A. Boetius, Anaerobic oxidation of methane: Progress with an unknown process. *Annu. Rev. Microbiol.* **63**, 311–334 (2009). Medline doi:10.1146/annurev.micro.61.080706.093130

12. P. R. Girguis, A. E. Cozen, E. F. DeLong, Growth and population dynamics of anaerobic methane-oxidizing archaea and sulfate-reducing bacteria in a continuous-flow bioreactor. *Appl. Environ. Microbiol.* **71**, 3725–3733 (2005). Medline doi:10.1128/AEM.71.7.3725-3733.2005

13. V. J. Orphan, K. A. Turk, A. M. Green, C. H. House, Patterns of ^{15}N assimilation and growth of methanotrophic ANME-2 archaea and sulfate-reducing bacteria within structured syntrophic consortia revealed by FISH-SIMS. *Environ.*

Microbiol. **11**, 1777–1791 (2009). Medline doi:10.1111/j.1462-2920.2009.01903.x

14. R. J. W. Meulepas, C. G. Jagersma, J. Gieteling, C. J. Buisman, A. J. Stams, P. N. Lens, Enrichment of anaerobic methanotrophs in sulfate-reducing membrane bioreactors. *Biotechnol. Bioeng.* **104**, 458–470 (2009). Medline doi:10.1002/bit.22412

15. T. Holler, F. Widdel, K. Knittel, R. Amann, M. Y. Kellermann, K. U. Hinrichs, A. Teske, A. Boetius, G. Wegener, Thermophilic anaerobic oxidation of methane by marine microbial consortia. *ISME J.* **5**, 1946–1956 (2011). Medline doi:10.1038/ismej.2011.77

16. K. Nauhaus, T. Treude, A. Boetius, M. Krüger, Environmental regulation of the anaerobic oxidation of methane: A comparison of ANME-I and ANME-II communities. *Environ. Microbiol.* **7**, 98–106 (2005). Medline doi:10.1111/j.1462-2920.2004.00669.x

17. K. Nauhaus, M. Albrecht, M. Elvert, A. Boetius, F. Widdel, In vitro cell growth of marine archaeal-bacterial consortia during anaerobic oxidation of methane with sulfate. *Environ. Microbiol.* **9**, 187–196 (2007). Medline doi:10.1111/j.1462-2920.2006.01127.x

18. S. B. Joye, A. Boetius, B. N. Orcutt, J. P. Montoya, H. N. Schulz, M. J. Erickson, S. K. Lugo, The anaerobic oxidation of methane and sulfate reduction in sediments from Gulf of Mexico cold seeps. *Chem. Geol.* **205**, 219–238 (2004). doi:10.1016/j.chemgeo.2003.12.019

19. A. Meyerdierks, M. Kube, I. Kostadinov, H. Teeling, F. O. Glöckner, R. Reinhardt, R. Amann, Metagenome and mRNA expression analyses of anaerobic methanotrophic archaea of the ANME-1 group. *Environ. Microbiol.* **12**, 422–439 (2010). Medline doi:10.1111/j.1462-2920.2009.02083.x

20. F. P. Wang, Y. Zhang, Y. Chen, Y. He, J. Qi, K. U. Hinrichs, X. X. Zhang, X. Xiao, N. Boon, Methanotrophic archaea possessing diverging methane-oxidizing and electron-transporting pathways. *ISME J.* **8**, 1069–1078 (2014). Medline doi:10.1038/ismej.2013.212

21. M. J. Alperin, T. M. Hoehler, Anaerobic methane oxidation by Archaea/sulfate-reducing bacteria aggregates: 1. Thermodynamic and physical constraints. *Am. J. Sci.* **309**, 869–957 (2009). doi:10.2475/10.2009.01

22. B. Orcutt, C. Meile, Constraints on mechanisms and rates of anaerobic oxidation of methane by microbial consortia: Process-based modeling of ANME-2 archaea and sulfate reducing bacteria interactions. *Biogeosciences* **5**, 1587–1599 (2008). doi:10.5194/bg-5-1587-2008

23. R. J. W. Meulepas, C. G. Jagersma, A. F. Khadem, A. J. M. Stams, P. N. L. Lens, Effect of methanogenic substrates on anaerobic oxidation of methane and sulfate reduction by an anaerobic methanotrophic enrichment. *Appl. Microbiol. Biotechnol.* **87**, 1499–1506 (2010). Medline doi:10.1007/s00253-010-2597-0

24. D. R. Bond, D. R. Lovley, Reduction of Fe(III) oxide by methanogens in the presence and absence of extracellular quinones. *Environ. Microbiol.* **4**, 115–124 (2002). Medline doi:10.1046/j.1462-2920.2002.00279.x

25. Additional supplementary information is available on *Science* Online.

26. L. G. Wilson, R. S. Bandurski, Enzymatic reactions involving sulfate, sulfite, selenate, and molybdate. *J. Biol. Chem.* **233**, 975–981 (1958). Medline

27. T. Holler, G. Wegener, H. Niemann, C. Deusner, T. G. Ferdelman, A. Boetius, B. Brunner, F. Widdel, Carbon and sulfur back flux during anaerobic microbial oxidation of methane and coupled sulfate reduction. *Proc. Natl. Acad. Sci. U.S.A.* **108**, E1484–E1490 (2011). Medline doi:10.1073/pnas.1106032108

28. M. Y. Yoshinaga, T. Holler, T. Goldhammer, G. Wegener, J. W. Pohlman, B. Brunner, M. M. M. Kuypers, K.-U. Hinrichs, M. Elvert, Carbon isotope equilibration during sulphate-limited anaerobic oxidation of methane. *Nat. Geosci.* **7**, 190–194 (2014). doi:10.1038/ngeo2069

29. S. Pirbadian, M. Y. El-Naggar, Multistep hopping and extracellular charge transfer in microbial redox chains. *Phys. Chem. Chem. Phys.* **14**, 13802–13808 (2012). Medline doi:10.1039/c2cp41185g

30. J. W. Voordeckers, B. C. Kim, M. Izallalen, D. R. Lovley, Role of *Geobacter sulfurreducens* outer surface c-type cytochromes in reduction of soil humic acid and anthraquinone-2,6-disulfonate. *Appl. Environ. Microbiol.* **76**, 2371–2375 (2010). Medline doi:10.1128/AEM.02250-09

31. K. Nauhaus, A. Boetius, M. Krüger, F. Widdel, In vitro demonstration of anaerobic oxidation of methane coupled to sulphate reduction in sediment from a marine gas hydrate area. *Environ. Microbiol.* **4**, 296–305 (2002). Medline doi:10.1046/j.1462-2920.2002.00299.x

32. J. J. Marlow, J. A. Steele, W. Ziebis, A. R. Thurber, L. A. Levin, V. J. Orphan, Carbonate-hosted methanotrophy represents an unrecognized methane sink in the deep sea. *Nat. Commun.* **5**, 5094 (2014). Medline doi:10.1038/ncomms6094

33. A. Green-Saxena, A. E. Dekas, N. F. Dalleska, V. J. Orphan, Nitrate-based niche differentiation by distinct sulfate-reducing bacteria involved in the anaerobic oxidation of methane. *ISME J.* **8**, 150–163 (2014). Medline doi:10.1038/ismej.2013.147

34. J. D. Cline, Spectrophotometric determination of hydrogen sulfide in natural waters. *Limnol. Oceanogr.* **14**, 454–458 (1969). doi:10.4319/lo.1969.14.3.0454

35. R. Gamage, A. J. McQuillan, B. M. Peake, Ultraviolet visible and electron-paramagnetic resonance spectroelectrochemical studies of the reduction products of some anthraquinone sulfonates in aqueous-solutions. *J. Chem. Soc., Faraday Trans.* **87**, 3653 (1991). doi:10.1039/ft9918703653

36. J. B. Conant, H. M. Kahn, L. F. Fieser, S. S. Kurtz Jr., An electrochemical study of the reversible reduction of organic compounds. *J. Am. Chem. Soc.* **44**, 1382–1396 (1922). doi:10.1021/ja01427a020

37. A. E. Dekas, G. L. Chadwick, M. W. Bowles, S. B. Joye, V. J. Orphan, Spatial distribution of nitrogen fixation in methane seep sediment and the role of the ANME archaea. *Environ. Microbiol.* **16**, 3012–3029 (2014). Medline doi:10.1111/1462-2920.12247

38. E. Trembath-Reichert, A. Green-Saxena, V. J. Orphan, in *Microbial Metagenomics, Metatranscriptomics, and Metaproteomics*, E. F. DeLong, Ed. (Elsevier Academic, San Diego, CA, 2013), vol. 531, pp. 2144.

39. C. Quast, E. Pruesse, P. Yilmaz, J. Gerken, T. Schweer, P. Yarza, J. Peplies, F. O. Glöckner, The SILVA ribosomal RNA gene database project: Improved data processing and web-based tools. *Nucleic Acids Res.* **41**, D590–D596 (2013). Medline doi:10.1093/nar/gks1219

40. S. F. Altschul, T. L. Madden, A. A. Schäffer, J. Zhang, Z. Zhang, W. Miller, D. J. Lipman, Gapped BLAST and PSI-BLAST: A new generation of protein database search programs. *Nucleic Acids Res.* **25**, 3389–3402 (1997). Medline doi:10.1093/nar/25.17.3389

41. W. Ludwig, O. Strunk, R. Westram, L. Richter, H. Meier, A. Yadhukumar, T. Buchner, S. Lai, G. Steppi, W. Jobb, I. Förster, S. Brettske, A. W. Gerber, O. Ginhart, S. Gross, S. Grumann, R. Hermann, A. Jost, T. König, R. Liss, M. Lüssmann, B. May, B. Nonhoff, R. Reichel, A. Strehlow, N. Stamatakis, A. Stuckmann, M. Vilbig, T. Lenke, A. Ludwig, K. H. Bode, Schleifer, ARB: A software environment for sequence data. *Nucleic Acids Res.* **32**, 1363–1371 (2004). Medline doi:10.1093/nar/gkh293

42. F. Ronquist, M. Teslenko, P. van der Mark, D. L. Ayres, A. Darling, S. Höhna, B. Larget, L. Liu, M. A. Suchard, J. P. Huelsenbeck, MrBayes 3.2: Efficient Bayesian phylogenetic inference and model choice across a large model space. *Syst. Biol.* **61**, 539–542 (2012). Medline doi:10.1093/sysbio/sys029

43. S. J. Hallam, P. R. Girguis, C. M. Preston, R. M. Richardson, E. F. Delong, Identification of methyl coenzyme M reductase A (mcrA) genes associated with methane-oxidizing archaea. *Appl. Environ. Microbiol.* **69**, 5483 (2003).

44. O. U. Mason, D. H. Case, T. H. Naehr, R. W. Lee, R. B. Thomas, J. V. Bailey, V. J. Orphan, Comparison of archaeal and bacterial diversity in methane seep carbonate nodules and host sediments, Eel River Basin and Hydrate Ridge, USA. *Microb. Ecol.* **70**, 766–784 (2015). Medline doi:10.1007/s00248-015-0615-6

45. J. G. Caporaso, J. Kuczynski, J. Stombaugh, K. Bittinger, F. D. Bushman, E. K. Costello, N. Fierer, A. G. Peña, J. K. Goodrich, J. I. Gordon, G. A. Huttley, S. T. Kelley, D. Knights, J. E. Koenig, R. E. Ley, C. A. Lozupone, D. McDonald, B. D. Muegge, M. Pirrung, J. Reeder, J. R. Sevinsky, P. J. Turnbaugh, W. A. Walters, J. Widmann, T. Yatsunenko, J. Zaneveld, R. Knight, QIIME allows analysis of high-throughput community sequencing data. *Nat. Methods* **7**, 335–336 (2010). Medline doi:10.1038/nmeth.f.303

46. B. M. Fuchs, J. Pernthaler, R. Amann, Single cell identifcation by fuorescence in situ hybridization. *Methods Gen. Molec. Microbiol.* **3**, 886 (2007).

47. R. I. Amann, L. Krumholz, D. A. Stahl, Fluorescent-oligonucleotide probing of whole cells for determinative, phylogenetic, and environmental studies in microbiology. *J. Bacteriol.* **172**, 762–770 (1990). Medline

48. K. Knittel, T. Lösekann, A. Boetius, R. Kort, R. Amann, Diversity and distribution of methanotrophic archaea at cold seeps. *Appl. Environ. Microbiol.* **71**, 467–479 (2005). Medline doi:10.1128/AEM.71.1.467-479.2005

49. W. Manz, M. Eisenbrecher, T. R. Neu, U. Szewzyk, Abundance and spatial organization of Gram-negative sulfate-reducing bacteria in activated sludge investigated by in situ probing with specific 16S rRNA targeted oligonucleotides. *FEMS Microbiol. Ecol.* **25**, 43–61 (1998). doi:10.1111/j.1574-6941.1998.tb00459.x

50. T. Lösekann, K. Knittel, T. Nadalig, B. Fuchs, H. Niemann, A. Boetius, R. Amann, Diversity and abundance of aerobic and anaerobic methane oxidizers at the Haakon Mosby Mud Volcano, Barents Sea. *Appl. Environ. Microbiol.* **73**, 3348–3362 (2007). Medline doi:10.1128/AEM.00016-07

51. L. Polerecky, B. Adam, J. Milucka, N. Musat, T. Vagner, M. M. Kuypers, Look@NanoSIMS—a tool for the analysis of nanoSIMS data in environmental microbiology. *Environ. Microbiol.* **14**, 1009–1023 (2012). Medline doi:10.1111/j.1462-2920.2011.02681.x

52. B. Thamdrup, Bacterial manganese and iron reduction in aquatic sediments. *Adv. Microb. Ecol.* **16**, 41–84 (2000). doi:10.1007/978-1-4615-4187-5_2

53. G. S. Wilson, Determination of oxidation-reduction potentials. *Methods Enzymol.* **54**, 396–410 (1978). Medline doi:10.1016/S0076-6879(78)54025-1

54. M. L. Fultz, R. A. Durst, Mediator compounds for the electrochemical study of biological redox systems - A compilation. *Anal. Chim. Acta* **140**, 1–18 (1982). doi:10.1016/S0003-2670(01)95447-9

55. R. S. Twigg, Oxidation-reduction aspects of resazurin. *Nature* **155**, 401–402 (1945). doi:10.1038/155401a0

56. M. Aeschbacher, D. Vergari, R. P. Schwarzenbach, M. Sander, Electrochemical analysis of proton and electron transfer equilibria of the reducible moieties in humic acids. *Environ. Sci. Technol.* **45**, 8385–8394 (2011). Medline doi:10.1021/es201981g

57. H. S. Mason, D. J. E. Ingram, B. Allen, The free radical property of melanins. *Arch. Biochem. Biophys.* **86**, 225–230 (1960). Medline doi:10.1016/0003-9861(60)90409-4